Validation of the MadAnalysis 5 implementation of ATLAS-SUSY-2014-10

Beranger Dumont (IBS-CTPU Daejeon)
beranger.dumont@lpsc.in2p3.fr

August 12, 2015

This note contains detailed validation material for the MadAnalysis 5 (MA5) implementation [1] of the ATLAS search for same-flavor opposite-sign dilepton pairs, jets, and large missing transverse momentum at the 8 TeV run of the LHC [2, 3]. Two different categories of signal regions (SRs) are considered in this search: the on-Z SRs, where 81 GeV $< m_{\ell\ell} <$ 101 GeV, and the off-Z SRs, where $m_{\ell\ell} <$ 80 GeV or $m_{\ell\ell} >$ 110 GeV. The on-Z SRs are designed to probe GGM scenarios where $\tilde{\chi}_1^0 \to (Z/h)\widetilde{G}$, while the results of the off-Z SRs are interpreted in simplified models where squarks or gluinos are pair-produced, and subsequently cascade decay into electroweak-inos and sleptons.

For the validation of the on-Z SRs, 200000 events are generated for the GGM benchmark scenario $(m_{\tilde{g}}, \mu) = (700, 200)$ GeV and $\tan\beta = 1.5$ with PYTHIA6 (standalone),[1] based on the SLHA file provided on HepData page [4]. All SUSY processes are generated (`MSEL=39`) but later on only gluino pair production, and all combination of electroweak-ino pair production are kept in order to follow the procedure considered in ATLAS [5]. Furthermore, we set `IMSS(11)=1` so that PYTHIA does not ignore the decay into gravitino.

The table for the decay of the lightest neutralino into gravitino has been added to the SLHA file given the branching fractions shown on Auxiliary Figure 1 of [3]. For the benchmark scenario $(m_{\tilde{g}}, \mu) = (700, 200)$ GeV and $\tan\beta = 1.5$, it reads $\mathcal{B}(\tilde{\chi}_1^0 \to \widetilde{G}\gamma) = 0.000028$, $\mathcal{B}(\tilde{\chi}_1^0 \to \widetilde{G}Z) = 0.989825$, and $\mathcal{B}(\tilde{\chi}_1^0 \to \widetilde{G}h) = 0.010147$ [5]. Moreover, as was done in ATLAS [5], we reweight the relative contributions of gluino pair production and electroweak-ino pair production according to the K-factors (we derive them using Prospino2 [6]).

Simplified models with squark or gluino pair production, used for the validation of the off-Z SRs, are generated with MadGraph 5 and PYTHIA6 following the explanations given in Section 3 of [2] (note that only left-handed charged sleptons are present in the cascade decay [5]). 100000 events are generated for each benchmark point.

For all cases, simulation of detector effects was done within `MadAnalysis 1.1.12beta`, using `delphesMA5tune` and a dedicated detector card [7] with a b-tagging efficiency of 60%. The number of events is scaled to the NLO cross sections given on Auxiliary Figure 1b, Auxiliary Figure 2b, and Auxiliary Figure 3b of the HepData page [4]. In the case of the GGM model,

[1] Thanks to Dipan Sengupta.

the cross sections which are given include all processes, although only gluino pair production and electroweak-ino pair production are effectively considered when generating events [5].

The next pages contain the cutflow tables and the kinematic distributions used for validation. Note that the signal regions SR-2j-btag and SR-4j-btag have not been validated since *i)* no cutflow table was made available, and *ii)* the kinematic distributions shown in Fig. 10 of [2, 3] are not readable and not provided in numerical form.

References

[1] Analysis code, doi: 10.7484/INSPIREHEP.DATA.RSTT.7HVX

[2] G. Aad *et al.* [ATLAS Collaboration], Eur. Phys. J. C **75** (2015) 7, 318 [arXiv:1503.03290 [hep-ex]].

[3] `https://atlas.web.cern.ch/Atlas/GROUPS/PHYSICS/PAPERS/SUSY-2014-10/`

[4] `hepdata.cedar.ac.uk/view/ins1351762`; see also `https://atlas.web.cern.ch/Atlas/GROUPS/PHYSICS/PAPERS/SUSY-2014-10/hepdata_info.pdf`

[5] Jamie Boyd, Tommaso Lari, Zachary Marshall, Emma Sian Kuwertz, and Benjamin Hooberman, private communication

[6] `http://www.thphys.uni-heidelberg.de/~plehn/index.php?show=prospino&visible=tools`

[7] `https://madanalysis.irmp.ucl.ac.be/attachment/wiki/PublicAnalysisDatabase/delphesMA5tune_card_ATLAS_2014_10.tcl`

1 Cutflows

1.1 GGM, $(m_{\tilde{g}}, \mu) = (700, 200)$ GeV

GGM, $(m_{\tilde{g}}, \mu) = (700, 200)$ GeV cutflow for SR Z ee				
cut	# events (scaled to σ and $\mathcal{L}$)	relative change	# events (official)	relative change (official)
Initial number of events	23142.0	23142.0		
2 OS ee	717.1	-96.9%	633.1	633.1
$n_j \geq 2$	386.8	-46.1%	369.4	-41.7%
electron crack veto	354.5	-8.4%	342.6	-7.3%
$m_{\ell\ell} > 15$ GeV	353.5	-0.3%	342.3	-0.1%
$\Delta\phi(j_1, E_T^{\text{miss}}) > 0.4$	331.4	-6.3%	323.5	-5.5%
$\Delta\phi(j_2, E_T^{\text{miss}}) > 0.4$	302.9	-8.6%	294.3	-9.0%
81 GeV $< m_{\ell\ell} <$ 101 GeV	222.2	-26.6%	244.4	-17.0%
$H_T > 600$ GeV	117.3	-47.2%	126.6	-48.2%
$E_T^{\text{miss}} > 225$ GeV	27.0	-77.0%	25.4	-79.9%

Table 1: Cutflow for the benchmark point GGM, $(m_{\tilde{g}}, \mu) = (700, 200)$ GeV in the SR Z ee.

GGM, $(m_{\tilde{g}}, \mu) = (700, 200)$ GeV cutflow for SR Z $\mu\mu$				
cut	# events (scaled to σ and $\mathcal{L}$)	relative change	# events (official)	relative change (official)
Initial number of events	23142.0	23142.0		
2 OS $\mu\mu$	696.0	-97.0%	609.7	609.7
$n_j \geq 2$	352.8	-49.3%	323.6	-46.9%
$m_{\ell\ell} > 15$ GeV	351.7	-0.3%	322.5	-0.3%
$\Delta\phi(j_1, E_T^{\text{miss}}) > 0.4$	332.8	-5.4%	302.6	-6.2%
$\Delta\phi(j_2, E_T^{\text{miss}}) > 0.4$	301.3	-9.5%	272.7	-9.9%
81 GeV $< m_{\ell\ell} <$ 101 GeV	242.7	-19.4%	230.6	-15.4%
$H_T > 600$ GeV	109.1	-55.0%	92.1	-60.1%
$E_T^{\text{miss}} > 225$ GeV	27.0	-75.3%	20.0	-78.3%

Table 2: Cutflow for the benchmark point GGM, $(m_{\tilde{g}}, \mu) = (700, 200)$ GeV in the SR Z $\mu\mu$.

1.2 $\tilde{g}\tilde{g}, (m_{\tilde{g}}, m_{\tilde{\chi}_1^0}) = (1025, 545)$ GeV

$\tilde{g}\tilde{g}, (m_{\tilde{g}}, m_{\tilde{\chi}_1^0}) = (1025, 545)$ GeV cutflow for SR above$Z$ ee, $4j$, b veto				
cut	# events (scaled to σ and $\mathcal{L}$)	relative change	# events (official)	relative change (official)
Initial number of events	395.9	395.9		
2 OS ee	33.9	-91.4%		
$p_T^{\ell 2} > 20$ GeV	33.5	-1.2%	35.1	35.1
$n_j \geq 2$	32.9	-1.8%	34.8	-0.9%
electron crack veto	30.8	-6.4%	32.4	-6.9%
$m_{\ell\ell} > 20$ GeV	30.6	-0.6%	32.2	-0.6%
$n_j \geq 4$	18.5	-39.5%	22.1	-31.4%
$E_T^{\text{miss}} > 200$ GeV	9.6	-48.1%	10.8	-51.1%
b-jet veto	7.3	-24.0%	7.9	-26.9%
$m_{\ell\ell} > 110$ GeV	5.4	-26.0%	5.7	-27.8%

Table 3: Cutflow for the benchmark point $\tilde{g}\tilde{g}, (m_{\tilde{g}}, m_{\tilde{\chi}_1^0}) = (1025, 545)$ GeV in the SR above$Z$ ee, $4j$, b veto.

$\tilde{g}\tilde{g}, (m_{\tilde{g}}, m_{\tilde{\chi}_1^0}) = (1025, 545)$ GeV cutflow for SR above$Z$ $\mu\mu$, $4j$, b veto				
cut	# events (scaled to σ and $\mathcal{L}$)	relative change	# events (official)	relative change (official)
Initial number of events	395.9	395.9		
2 OS $\mu\mu$	27.8	-93.0%		
$p_T^{\ell 2} > 20$ GeV	27.5	-1.1%	26.0	26.0
$n_j \geq 2$	27.3	-0.7%	25.7	-1.2%
$m_{\ell\ell} > 20$ GeV	27.1	-0.7%	25.7	-0.0%
$n_j \geq 4$	17.1	-36.9%	18.3	-28.8%
$E_T^{\text{miss}} > 200$ GeV	8.7	-49.1%	9.1	-50.3%
b-jet veto	6.5	-25.3%	6.6	-27.5%
$m_{\ell\ell} > 110$ GeV	4.9	-24.6%	4.9	-25.8%

Table 4: Cutflow for the benchmark point $\tilde{g}\tilde{g}, (m_{\tilde{g}}, m_{\tilde{\chi}_1^0}) = (1025, 545)$ GeV in the SR above$Z$ $\mu\mu$, $4j$, b veto.

$\tilde{g}\tilde{g}, (m_{\tilde{g}}, m_{\tilde{\chi}_1^0}) = (1025, 545)$ GeV cutflow for SR below$Z$ ee, $4j$, b veto				
cut	# events (scaled to σ and $\mathcal{L}$)	relative change	# events (official)	relative change (official)
Initial number of events	395.9	395.9		
2 OS ee	33.9	-91.4%		
$p_T^{\ell 2} > 20$ GeV	33.5	-1.2%	35.1	35.1
$n_j \geq 2$	32.9	-1.8%	34.8	-0.9%
electron crack veto	30.8	-6.4%	32.4	-6.9%
$m_{\ell\ell} > 20$ GeV	30.6	-0.6%	32.2	-0.6%
$n_j \geq 4$	18.5	-39.5%	22.1	-31.4%
$E_T^{\text{miss}} > 200$ GeV	9.6	-48.1%	10.8	-51.1%
b-jet veto	7.3	-24.0%	7.9	-26.9%
20 GeV $< m_{\ell\ell} <$ 80 GeV	1.1	-84.9%	1.2	-84.8%

Table 5: Cutflow for the benchmark point $\tilde{g}\tilde{g}, (m_{\tilde{g}}, m_{\tilde{\chi}_1^0}) = (1025, 545)$ GeV in the SR below$Z$ ee, $4j$, b veto.

$\tilde{g}\tilde{g}, (m_{\tilde{g}}, m_{\tilde{\chi}_1^0}) = (1025, 545)$ GeV cutflow for SR below$Z$ $\mu\mu,\ 4j,\ b$ veto				
cut	# events (scaled to σ and $\mathcal{L}$)	relative change	# events (official)	relative change (official)
Initial number of events	395.9	395.9		
2 OS $\mu\mu$	27.8	-93.0%		
$p_T^{\ell 2} > 20$ GeV	27.5	-1.1%	26.0	26.0
$n_j \geq 2$	27.3	-0.7%	25.7	-1.2%
$m_{\ell\ell} > 20$ GeV	27.1	-0.7%	25.7	-0.0%
$n_j \geq 4$	17.1	-36.9%	18.3	-28.8%
$E_T^{\text{miss}} > 200$ GeV	8.7	-49.1%	9.1	-50.3%
b-jet veto	6.5	-25.3%	6.6	-27.5%
20 GeV $< m_{\ell\ell} <$ 80 GeV	0.9	-86.2%	0.9	-86.4%

Table 6: Cutflow for the benchmark point $\tilde{g}\tilde{g}, (m_{\tilde{g}}, m_{\tilde{\chi}_1^0}) = (1025, 545)$ GeV in the SR below$Z$ $\mu\mu,\ 4j,\ b$ veto.

1.3 $\tilde{g}\tilde{g}, (m_{\tilde{g}}, m_{\tilde{\chi}_1^0}) = (1185, 65)$ GeV

$\tilde{g}\tilde{g}, (m_{\tilde{g}}, m_{\tilde{\chi}_1^0}) = (1185, 65)$ GeV cutflow for SR above$Z$ ee, $4j$, b veto				
cut	# events (scaled to σ and $\mathcal{L}$)	relative change	# events (official)	relative change (official)
Initial number of events	101.5	101.5		
2 OS ee	9.3	-90.8%		
$p_T^{\ell 2} > 20$ GeV	9.3	-0.0%	9.9	9.9
$n_j \geq 2$	9.3	-0.0%	9.9	-0.0%
electron crack veto	8.6	-7.5%	9.3	-6.1%
$m_{\ell\ell} > 20$ GeV	8.6	-0.0%	9.3	-0.0%
$n_j \geq 4$	7.3	-15.1%	8.2	-11.8%
$E_T^{\text{miss}} > 200$ GeV	5.5	-24.7%	6.1	-25.6%
b-jet veto	4.0	-27.3%	4.4	-27.9%
$m_{\ell\ell} > 110$ GeV	3.8	-5.0%	4.2	-4.5%

Table 7: Cutflow for the benchmark point $\tilde{g}\tilde{g}, (m_{\tilde{g}}, m_{\tilde{\chi}_1^0}) = (1185, 65)$ GeV in the SR above$Z$ ee, $4j$, b veto.

$\tilde{g}\tilde{g}, (m_{\tilde{g}}, m_{\tilde{\chi}_1^0}) = (1185, 65)$ GeV cutflow for SR above$Z$ $\mu\mu,\ 4j,\ b$ veto				
cut	# events (scaled to σ and $\mathcal{L}$)	relative change	# events (official)	relative change (official)
Initial number of events	101.5	101.5		
2 OS $\mu\mu$	6.9	-93.2%		
$p_T^{\ell 2} > 20$ GeV	6.8	-1.4%	6.4	6.4
$n_j \geq 2$	6.8	-0.0%	6.3	-1.6%
$m_{\ell\ell} > 20$ GeV	6.8	-0.0%	6.3	-0.0%
$n_j \geq 4$	5.9	-13.2%	5.8	-7.9%
$E_T^{\text{miss}} > 200$ GeV	4.3	-27.1%	4.2	-27.6%
b-jet veto	3.1	-27.9%	3.1	-26.2%
$m_{\ell\ell} > 110$ GeV	3.0	-3.2%	3.0	-3.2%

Table 8: Cutflow for the benchmark point $\tilde{g}\tilde{g}, (m_{\tilde{g}}, m_{\tilde{\chi}_1^0}) = (1185, 65)$ GeV in the SR above$Z$ $\mu\mu,\ 4j,\ b$ veto.

$\tilde{g}\tilde{g}, (m_{\tilde{g}}, m_{\tilde{\chi}_1^0}) = (1185, 65)$ GeV cutflow for SR below$Z$ $ee,\ 4j,\ b$ veto				
cut	# events (scaled to σ and $\mathcal{L}$)	relative change	# events (official)	relative change (official)
Initial number of events	101.5	101.5		
2 OS ee	9.3	-90.8%		
$p_T^{\ell 2} > 20$ GeV	9.3	-0.0%	9.9	9.9
$n_j \geq 2$	9.3	-0.0%	9.9	-0.0%
electron crack veto	8.6	-7.5%	9.3	-6.1%
$m_{\ell\ell} > 20$ GeV	8.6	-0.0%	9.3	-0.0%
$n_j \geq 4$	7.3	-15.1%	8.2	-11.8%
$E_T^{\text{miss}} > 200$ GeV	5.5	-24.7%	6.1	-25.6%
b-jet veto	4.0	-27.3%	4.4	-27.9%
20 GeV $< m_{\ell\ell} <$ 80 GeV	0.1	-97.5%	0.1	-97.7%

Table 9: Cutflow for the benchmark point $\tilde{g}\tilde{g}, (m_{\tilde{g}}, m_{\tilde{\chi}_1^0}) = (1185, 65)$ GeV in the SR below$Z$ $ee,\ 4j,\ b$ veto.

$\tilde{g}\tilde{g}, (m_{\tilde{g}}, m_{\tilde{\chi}_1^0}) = (1185, 65)$ GeV cutflow for SR below$Z$ $\mu\mu,\ 4j,\ b$ veto				
cut	# events (scaled to σ and $\mathcal{L}$)	relative change	# events (official)	relative change (official)
Initial number of events	101.5	101.5		
2 OS $\mu\mu$	6.9	-93.2%		
$p_T^{\ell 2} > 20$ GeV	6.8	-1.4%	6.4	6.4
$n_j \geq 2$	6.8	-0.0%	6.3	-1.6%
$m_{\ell\ell} > 20$ GeV	6.8	-0.0%	6.3	-0.0%
$n_j \geq 4$	5.9	-13.2%	5.8	-7.9%
$E_T^{\text{miss}} > 200$ GeV	4.3	-27.1%	4.2	-27.6%
b-jet veto	3.1	-27.9%	3.1	-26.2%
20 GeV $< m_{\ell\ell} <$ 80 GeV	0.1	-96.8%	0.1	-96.8%

Table 10: Cutflow for the benchmark point $\tilde{g}\tilde{g}, (m_{\tilde{g}}, m_{\tilde{\chi}_1^0}) = (1185, 65)$ GeV in the SR below$Z$ $\mu\mu,\ 4j,\ b$ veto.

1.4 $\tilde{g}\tilde{g}, (m_{\tilde{g}}, m_{\tilde{\chi}_1^0}) = (825, 585)$ GeV

$\tilde{g}\tilde{g}, (m_{\tilde{g}}, m_{\tilde{\chi}_1^0}) = (825, 585)$ GeV cutflow for SR above$Z$ ee, $4j$, b veto				
cut	# events (scaled to σ and $\mathcal{L}$)	relative change	# events (official)	relative change (official)
Initial number of events	2501.0	2501.0		
2 OS ee	186.3	-92.6%		
$p_T^{\ell 2} > 20$ GeV	173.7	-6.8%	168.0	168.0
$n_j \geq 2$	152.2	-12.4%	157.0	-6.5%
electron crack veto	142.6	-6.3%	144.9	-7.7%
$m_{\ell\ell} > 20$ GeV	138.7	-2.7%	142.5	-1.7%
$n_j \geq 4$	44.2	-68.1%	58.0	-59.3%
$E_T^{\text{miss}} > 200$ GeV	16.0	-63.8%	17.5	-69.8%
b-jet veto	12.3	-23.1%	13.3	-24.0%
$m_{\ell\ell} > 110$ GeV	2.2	-82.1%	2.2	-83.5%

Table 11: Cutflow for the benchmark point $\tilde{g}\tilde{g}, (m_{\tilde{g}}, m_{\tilde{\chi}_1^0}) = (825, 585)$ GeV in the SR above$Z$ ee, $4j$, b veto.

$\tilde{g}\tilde{g}, (m_{\tilde{g}}, m_{\tilde{\chi}_1^0}) = (825, 585)$ GeV cutflow for SR above$Z$ $\mu\mu,\ 4j,\ b$ veto				
cut	# events (scaled to σ and $\mathcal{L}$)	relative change	# events (official)	relative change (official)
Initial number of events	2501.0	2501.0		
2 OS $\mu\mu$	184.3	-92.6%		
$p_T^{\ell 2} > 20$ GeV	170.8	-7.3%	157.4	157.4
$n_j \geq 2$	151.5	-11.3%	145.5	-7.6%
$m_{\ell\ell} > 20$ GeV	146.7	-3.2%	143.2	-1.6%
$n_j \geq 4$	49.6	-66.2%	58.2	-59.4%
$E_T^{\text{miss}} > 200$ GeV	17.9	-63.9%	18.0	-69.1%
b-jet veto	14.4	-19.6%	14.2	-21.1%
$m_{\ell\ell} > 110$ GeV	2.9	-79.9%	2.5	-82.4%

Table 12: Cutflow for the benchmark point $\tilde{g}\tilde{g}, (m_{\tilde{g}}, m_{\tilde{\chi}_1^0}) = (825, 585)$ GeV in the SR above$Z$ $\mu\mu,\ 4j,\ b$ veto.

$\tilde{g}\tilde{g}, (m_{\tilde{g}}, m_{\tilde{\chi}_1^0}) = (825, 585)$ GeV cutflow for SR below$Z$ $ee,\ 4j,\ b$ veto				
cut	# events (scaled to σ and $\mathcal{L}$)	relative change	# events (official)	relative change (official)
Initial number of events	2501.0	2501.0		
2 OS ee	186.3	-92.6%		
$p_T^{\ell 2} > 20$ GeV	173.7	-6.8%	168.0	168.0
$n_j \geq 2$	152.2	-12.4%	157.0	-6.5%
electron crack veto	142.6	-6.3%	144.9	-7.7%
$m_{\ell\ell} > 20$ GeV	138.7	-2.7%	142.5	-1.7%
$n_j \geq 4$	44.2	-68.1%	58.0	-59.3%
$E_T^{\text{miss}} > 200$ GeV	16.0	-63.8%	17.5	-69.8%
b-jet veto	12.3	-23.1%	13.3	-24.0%
20 GeV $< m_{\ell\ell} <$ 80 GeV	5.2	-57.7%	5.7	-57.1%

Table 13: Cutflow for the benchmark point $\tilde{g}\tilde{g}, (m_{\tilde{g}}, m_{\tilde{\chi}_1^0}) = (825, 585)$ GeV in the SR below$Z$ $ee,\ 4j,\ b$ veto.

$\tilde{g}\tilde{g}, (m_{\tilde{g}}, m_{\tilde{\chi}_1^0}) = (825, 585)$ GeV cutflow for SR below$Z$ $\mu\mu,\ 4j,\ b$ veto				
cut	# events (scaled to σ and $\mathcal{L}$)	relative change	# events (official)	relative change (official)
Initial number of events	2501.0	2501.0		
2 OS $\mu\mu$	184.3	-92.6%		
$p_T^{\ell 2} > 20$ GeV	170.8	-7.3%	157.4	157.4
$n_j \geq 2$	151.5	-11.3%	145.5	-7.6%
$m_{\ell\ell} > 20$ GeV	146.7	-3.2%	143.2	-1.6%
$n_j \geq 4$	49.6	-66.2%	58.2	-59.4%
$E_T^{\text{miss}} > 200$ GeV	17.9	-63.9%	18.0	-69.1%
b-jet veto	14.4	-19.6%	14.2	-21.1%
20 GeV $< m_{\ell\ell} <$ 80 GeV	6.6	-54.2%	7.1	-50.0%

Table 14: Cutflow for the benchmark point $\tilde{g}\tilde{g}, (m_{\tilde{g}}, m_{\tilde{\chi}_1^0}) = (825, 585)$ GeV in the SR below$Z$ $\mu\mu,\ 4j,\ b$ veto.

1.5 $\tilde{q}\tilde{q}, (m_{\tilde{q}}, m_{\tilde{\chi}_1^0}) = (545, 385)$ GeV

$\tilde{q}\tilde{q}, (m_{\tilde{q}}, m_{\tilde{\chi}_1^0}) = (545, 385)$ GeV cutflow for SR above$Z$ $ee,\ 2j,\ b$ veto				
cut	# events (scaled to σ and $\mathcal{L}$)	relative change	# events (official)	relative change (official)
Initial number of events	3859.0	3859.0		
2 OS ee	278.1	-92.8%		
$p_T^{\ell 2} > 20$ GeV	230.7	-17.0%	205.7	205.7
$n_j \geq 2$	178.6	-22.6%	172.8	-16.0%
electron crack veto	167.3	-6.3%	162.2	-6.1%
$m_{\ell\ell} > 20$ GeV	155.5	-7.1%	154.1	-5.0%
$E_T^{\text{miss}} > 200$ GeV	29.4	-81.1%	26.3	-82.9%
b-jet veto	24.8	-15.6%	23.0	-12.5%
$m_{\ell\ell} > 110$ GeV	1.5	-94.0%	2.0	-91.3%

Table 15: Cutflow for the benchmark point $\tilde{q}\tilde{q}, (m_{\tilde{q}}, m_{\tilde{\chi}_1^0}) = (545, 385)$ GeV in the SR above$Z$ $ee,\ 2j,\ b$ veto.

$\tilde{q}\tilde{q}, (m_{\tilde{q}}, m_{\tilde{\chi}_1^0}) = (545, 385)$ GeV cutflow for SR above$Z$ $\mu\mu,\ 2j,\ b$ veto				
cut	# events (scaled to σ and $\mathcal{L}$)	relative change	# events (official)	relative change (official)
Initial number of events	3859.0	3859.0		
2 OS $\mu\mu$	319.3	-91.7%		
$p_T^{\ell 2} > 20$ GeV	263.4	-17.5%	234.5	234.5
$n_j \geq 2$	206.9	-21.5%	197.9	-15.6%
$m_{\ell\ell} > 20$ GeV	193.0	-6.7%	187.2	-5.4%
$E_T^{\text{miss}} > 200$ GeV	32.4	-83.2%	27.4	-85.4%
b-jet veto	26.3	-18.8%	22.5	-17.9%
$m_{\ell\ell} > 110$ GeV	1.4	-94.7%	1.1	-95.1%

Table 16: Cutflow for the benchmark point $\tilde{q}\tilde{q}, (m_{\tilde{q}}, m_{\tilde{\chi}_1^0}) = (545, 385)$ GeV in the SR above$Z$ $\mu\mu,\ 2j,\ b$ veto.

$\tilde{q}\tilde{q}, (m_{\tilde{q}}, m_{\tilde{\chi}_1^0}) = (545, 385)$ GeV cutflow for SR below$Z$ $ee,\ 2j,\ b$ veto				
cut	# events (scaled to σ and $\mathcal{L}$)	relative change	# events (official)	relative change (official)
Initial number of events	3859.0	3859.0		
2 OS ee	278.1	-92.8%		
$p_T^{\ell 2} > 20$ GeV	230.7	-17.0%	205.7	205.7
$n_j \geq 2$	178.6	-22.6%	172.8	-16.0%
electron crack veto	167.3	-6.3%	162.2	-6.1%
$m_{\ell\ell} > 20$ GeV	155.5	-7.1%	154.1	-5.0%
$E_T^{\text{miss}} > 200$ GeV	29.4	-81.1%	26.3	-82.9%
b-jet veto	24.8	-15.6%	23.0	-12.5%
20 GeV $< m_{\ell\ell} <$ 80 GeV	21.0	-15.3%	18.9	-17.8%

Table 17: Cutflow for the benchmark point $\tilde{q}\tilde{q}, (m_{\tilde{q}}, m_{\tilde{\chi}_1^0}) = (545, 385)$ GeV in the SR below$Z$ $ee,\ 2j,\ b$ veto.

$\tilde{q}\tilde{q}, (m_{\tilde{q}}, m_{\tilde{\chi}_1^0}) = (545, 385)$ GeV cutflow for SR below$Z$ $\mu\mu,\ 2j,\ b$ veto				
cut	# events (scaled to σ and $\mathcal{L}$)	relative change	# events (official)	relative change (official)
Initial number of events	3859.0	3859.0		
2 OS $\mu\mu$	319.3	-91.7%		
$p_T^{\ell 2} > 20$ GeV	263.4	-17.5%	234.5	234.5
$n_j \geq 2$	206.9	-21.5%	197.9	-15.6%
$m_{\ell\ell} > 20$ GeV	193.0	-6.7%	187.2	-5.4%
$E_T^{\text{miss}} > 200$ GeV	32.4	-83.2%	27.4	-85.4%
b-jet veto	26.3	-18.8%	22.5	-17.9%
20 GeV $< m_{\ell\ell} <$ 80 GeV	22.9	-12.9%	18.9	-16.0%

Table 18: Cutflow for the benchmark point $\tilde{q}\tilde{q}, (m_{\tilde{q}}, m_{\tilde{\chi}_1^0}) = (545, 385)$ GeV in the SR below$Z$ $\mu\mu,\ 2j,\ b$ veto.

1.6 $\tilde{q}\tilde{q}, (m_{\tilde{q}}, m_{\tilde{\chi}_1^0}) = (665, 265)$ GeV

$\tilde{q}\tilde{q}, (m_{\tilde{q}}, m_{\tilde{\chi}_1^0}) = (665, 265)$ GeV cutflow for SR above$Z$ $ee,\ 2j,\ b$ veto				
cut	# events (scaled to σ and $\mathcal{L}$)	relative change	# events (official)	relative change (official)
Initial number of events	948.0	948.0		
2 OS ee	89.3	-90.6%		
$p_T^{\ell 2} > 20$ GeV	87.5	-2.0%	91.9	91.9
$n_j \geq 2$	81.8	-6.5%	88.5	-3.7%
electron crack veto	75.8	-7.3%	83.0	-6.2%
$m_{\ell\ell} > 20$ GeV	75.0	-1.1%	82.6	-0.5%
$E_T^{\text{miss}} > 200$ GeV	35.1	-53.2%	36.9	-55.3%
b-jet veto	29.8	-15.1%	31.3	-15.2%
$m_{\ell\ell} > 110$ GeV	19.7	-33.9%	20.8	-33.5%

Table 19: Cutflow for the benchmark point $\tilde{q}\tilde{q}, (m_{\tilde{q}}, m_{\tilde{\chi}_1^0}) = (665, 265)$ GeV in the SR above$Z$ $ee,\ 2j,\ b$ veto.

$\tilde{q}\tilde{q}, (m_{\tilde{q}}, m_{\tilde{\chi}_1^0}) = (665, 265)$ GeV cutflow for SR above$Z$ $\mu\mu,\ 2j,\ b$ veto				
cut	# events (scaled to σ and $\mathcal{L}$)	relative change	# events (official)	relative change (official)
Initial number of events	948.0	948.0		
2 OS $\mu\mu$	85.8	-90.9%		
$p_T^{\ell 2} > 20$ GeV	83.7	-2.4%	81.9	81.9
$n_j \geq 2$	79.1	-5.5%	79.2	-3.3%
$m_{\ell\ell} > 20$ GeV	78.2	-1.1%	79.0	-0.3%
$E_T^{\text{miss}} > 200$ GeV	36.0	-54.0%	36.4	-53.9%
b-jet veto	30.8	-14.4%	29.9	-17.9%
$m_{\ell\ell} > 110$ GeV	21.3	-30.8%	20.1	-32.8%

Table 20: Cutflow for the benchmark point $\tilde{q}\tilde{q}, (m_{\tilde{q}}, m_{\tilde{\chi}_1^0}) = (665, 265)$ GeV in the SR above$Z$ $\mu\mu,\ 2j,\ b$ veto.

$\tilde{q}\tilde{q}, (m_{\tilde{q}}, m_{\tilde{\chi}_1^0}) = (665, 265)$ GeV cutflow for SR below$Z$ $ee,\ 2j,\ b$ veto				
cut	# events (scaled to σ and $\mathcal{L}$)	relative change	# events (official)	relative change (official)
Initial number of events	948.0	948.0		
2 OS ee	89.3	-90.6%		
$p_T^{\ell 2} > 20$ GeV	87.5	-2.0%	91.9	91.9
$n_j \geq 2$	81.8	-6.5%	88.5	-3.7%
electron crack veto	75.8	-7.3%	83.0	-6.2%
$m_{\ell\ell} > 20$ GeV	75.0	-1.1%	82.6	-0.5%
$E_T^{\text{miss}} > 200$ GeV	35.1	-53.2%	36.9	-55.3%
b-jet veto	29.8	-15.1%	31.3	-15.2%
20 GeV $< m_{\ell\ell} <$ 80 GeV	5.4	-81.9%	5.5	-82.4%

Table 21: Cutflow for the benchmark point $\tilde{q}\tilde{q}, (m_{\tilde{q}}, m_{\tilde{\chi}_1^0}) = (665, 265)$ GeV in the SR below$Z$ $ee,\ 2j,\ b$ veto.

$\tilde{q}\tilde{q}, (m_{\tilde{q}}, m_{\tilde{\chi}_1^0}) = (665, 265)$ GeV cutflow for SR below$Z$ $\mu\mu,\ 2j,\ b$ veto				
cut	# events (scaled to σ and $\mathcal{L}$)	relative change	# events (official)	relative change (official)
Initial number of events	948.0	948.0		
2 OS $\mu\mu$	85.8	-90.9%		
$p_T^{\ell 2} > 20$ GeV	83.7	-2.4%	81.9	81.9
$n_j \geq 2$	79.1	-5.5%	79.2	-3.3%
$m_{\ell\ell} > 20$ GeV	78.2	-1.1%	79.0	-0.3%
$E_T^{\text{miss}} > 200$ GeV	36.0	-54.0%	36.4	-53.9%
b-jet veto	30.8	-14.4%	29.9	-17.9%
20 GeV $< m_{\ell\ell} <$ 80 GeV	5.0	-83.8%	4.9	-83.6%

Table 22: Cutflow for the benchmark point $\tilde{q}\tilde{q}, (m_{\tilde{q}}, m_{\tilde{\chi}_1^0}) = (665, 265)$ GeV in the SR below$Z$ $\mu\mu,\ 2j,\ b$ veto.

1.7 $\tilde{q}\tilde{q}, (m_{\tilde{q}}, m_{\tilde{\chi}_1^0}) = (475, 25)$ GeV

$\tilde{q}\tilde{q}, (m_{\tilde{q}}, m_{\tilde{\chi}_1^0}) = (475, 25)$ GeV cutflow for SR above$Z$ $ee,\ 2j,\ b$ veto				
cut	# events (scaled to σ and $\mathcal{L}$)	relative change	# events (official)	relative change (official)
Initial number of events	404.0	404.0		
2 OS ee	40.6	-90.0%		
$p_T^{\ell 2} > 20$ GeV	40.0	-1.5%	42.2	42.2
$n_j \geq 2$	38.4	-4.0%	41.1	-2.6%
electron crack veto	35.6	-7.3%	38.4	-6.6%
$m_{\ell\ell} > 20$ GeV	35.5	-0.3%	38.4	-0.0%
$E_T^{\text{miss}} > 200$ GeV	22.6	-36.3%	23.9	-37.8%
b-jet veto	18.9	-16.4%	19.8	-17.2%
$m_{\ell\ell} > 110$ GeV	16.5	-12.7%	17.5	-11.6%

Table 23: Cutflow for the benchmark point $\tilde{q}\tilde{q}, (m_{\tilde{q}}, m_{\tilde{\chi}_1^0}) = (475, 25)$ GeV in the SR above$Z$ $ee,\ 2j,\ b$ veto.

$\tilde{q}\tilde{q}, (m_{\tilde{q}}, m_{\tilde{\chi}_1^0}) = (475, 25)$ GeV cutflow for SR above$Z$ $\mu\mu,\ 2j,\ b$ veto				
cut	# events (scaled to σ and $\mathcal{L}$)	relative change	# events (official)	relative change (official)
Initial number of events	404.0	404.0		
2 OS $\mu\mu$	36.1	-91.1%		
$p_T^{\ell 2} > 20$ GeV	35.5	-1.7%	33.4	33.4
$n_j \geq 2$	34.2	-3.7%	32.6	-2.4%
$m_{\ell\ell} > 20$ GeV	34.0	-0.6%	32.5	-0.3%
$E_T^{\text{miss}} > 200$ GeV	21.7	-36.2%	20.7	-36.3%
b-jet veto	18.2	-16.1%	16.7	-19.3%
$m_{\ell\ell} > 110$ GeV	16.0	-12.1%	14.7	-12.0%

Table 24: Cutflow for the benchmark point $\tilde{q}\tilde{q}, (m_{\tilde{q}}, m_{\tilde{\chi}_1^0}) = (475, 25)$ GeV in the SR above$Z$ $\mu\mu,\ 2j,\ b$ veto.

$\tilde{q}\tilde{q}, (m_{\tilde{q}}, m_{\tilde{\chi}_1^0}) = (475, 25)$ GeV cutflow for SR below$Z$ $ee,\ 2j,\ b$ veto				
cut	# events (scaled to σ and $\mathcal{L}$)	relative change	# events (official)	relative change (official)
Initial number of events	404.0	404.0		
2 OS ee	40.6	-90.0%		
$p_T^{\ell 2} > 20$ GeV	40.0	-1.5%	42.2	42.2
$n_j \geq 2$	38.4	-4.0%	41.1	-2.6%
electron crack veto	35.6	-7.3%	38.4	-6.6%
$m_{\ell\ell} > 20$ GeV	35.5	-0.3%	38.4	-0.0%
$E_T^{\text{miss}} > 200$ GeV	22.6	-36.3%	23.9	-37.8%
b-jet veto	18.9	-16.4%	19.8	-17.2%
20 GeV $< m_{\ell\ell} <$ 80 GeV	1.3	-93.1%	1.2	-93.9%

Table 25: Cutflow for the benchmark point $\tilde{q}\tilde{q}, (m_{\tilde{q}}, m_{\tilde{\chi}_1^0}) = (475, 25)$ GeV in the SR below$Z$ $ee,\ 2j,\ b$ veto.

$\tilde{q}\tilde{q}, (m_{\tilde{q}}, m_{\tilde{\chi}_1^0}) = (475, 25)$ GeV cutflow for SR below$Z$ $\mu\mu,\ 2j,\ b$ veto				
cut	# events (scaled to σ and $\mathcal{L}$)	relative change	# events (official)	relative change (official)
Initial number of events	404.0	404.0		
2 OS $\mu\mu$	36.1	-91.1%		
$p_T^{\ell 2} > 20$ GeV	35.5	-1.7%	33.4	33.4
$n_j \geq 2$	34.2	-3.7%	32.6	-2.4%
$m_{\ell\ell} > 20$ GeV	34.0	-0.6%	32.5	-0.3%
$E_T^{\text{miss}} > 200$ GeV	21.7	-36.2%	20.7	-36.3%
b-jet veto	18.2	-16.1%	16.7	-19.3%
20 GeV $< m_{\ell\ell} <$ 80 GeV	1.2	-93.4%	0.9	-94.6%

Table 26: Cutflow for the benchmark point $\tilde{q}\tilde{q}, (m_{\tilde{q}}, m_{\tilde{\chi}_1^0}) = (475, 25)$ GeV in the SR below$Z$ $\mu\mu,\ 2j,\ b$ veto.

2 Histograms

In the histograms below, the solid lines correspond to the results from the MadAnalysis 5 implementation, while the dashed lines are the official ATLAS results. They correspond to Figs. 6, 7, 8, and 9 of [2, 3]. In the case of Fig. 6 and Fig. 9, the number of events for the benchmark SUSY scenarios is provided in numerical form on the HepData page [4]. As it is not the case for Fig. 7 and 8, we extract the number of events from the figure. Note that the $m_{\ell\ell}$ distributions for the b-tagged SRs, shown in Fig. 10 of [2, 3], are not reproduced since the number of events for the benchmark scenarios is not available on HepData, and the extraction from the figure would come with a large uncertainty given the scale.

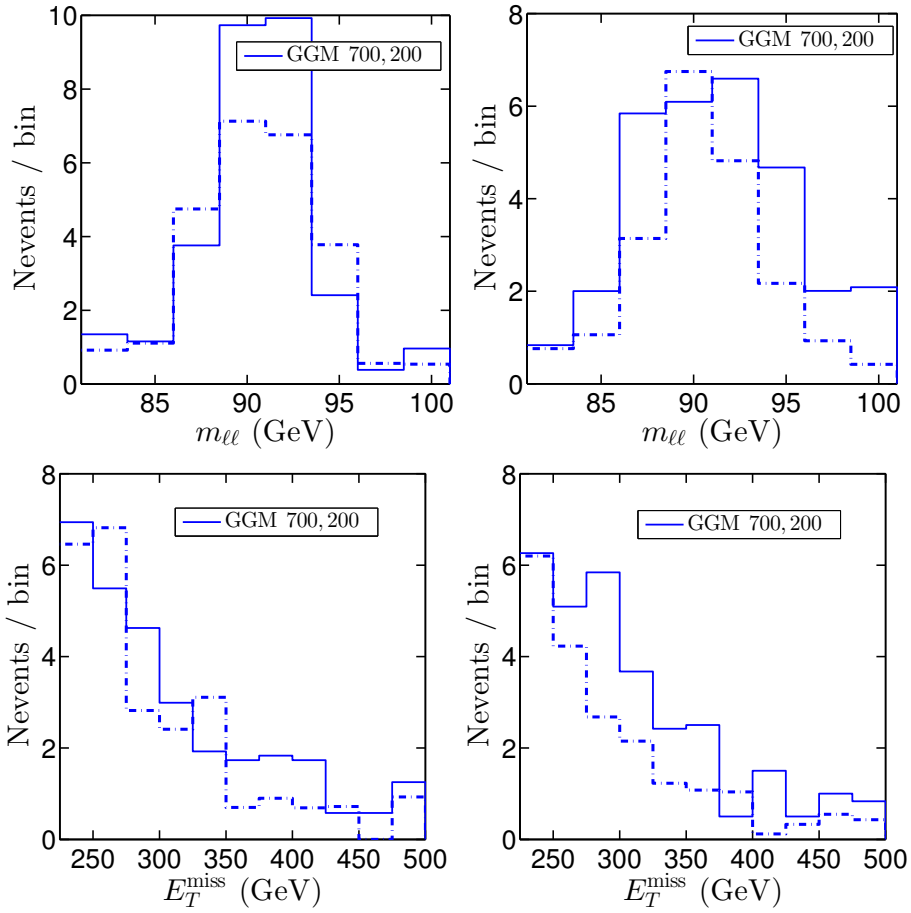

Figure 1: $m_{\ell\ell}$ (top row) and $E_T^{\rm miss}$ (bottom row) distributions in the Z ee (left) and Z $\mu\mu$ (right) SRs, after all cuts. Corresponds to Fig. 6 of [2, 3].

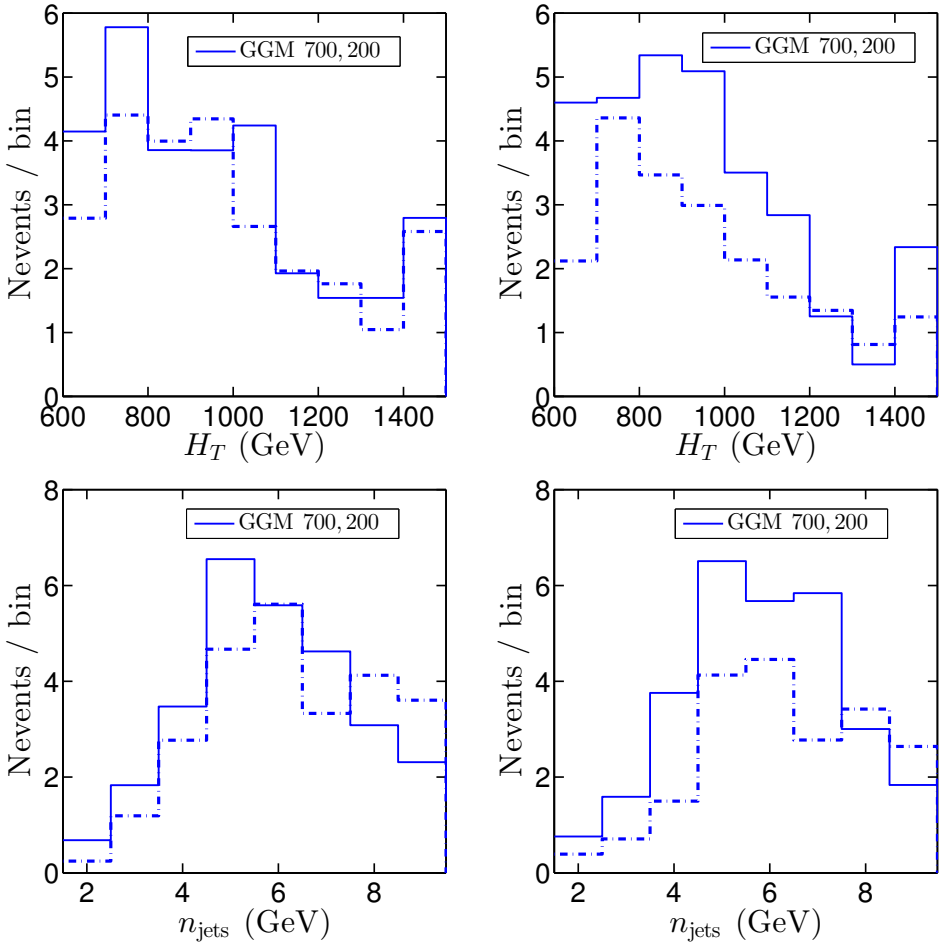

Figure 2: H_T (top row) and n_{jets} (bottom row) distributions in the Z ee (left) and Z $\mu\mu$ (right) SRs, after all cuts. Corresponds to Fig. 7 of [2,3].

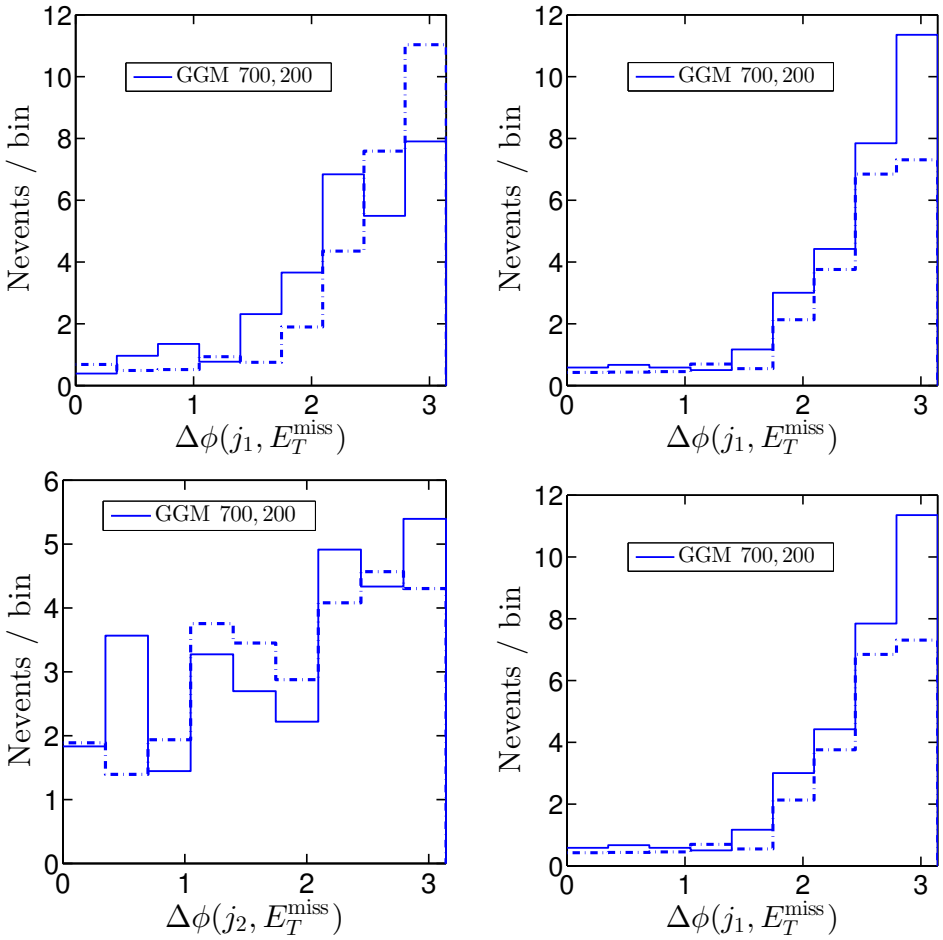

Figure 3: $\Delta\phi(j_1, E_T^{\rm miss})$ (top row) and $\Delta\phi(j_2, E_T^{\rm miss})$ (bottom row) distributions in the Z ee (left) and Z $\mu\mu$ (right) SRs, after all cuts except the ones on $\Delta\phi(j_2, E_T^{\rm miss})$ and $\Delta\phi(j_2, E_T^{\rm miss})$. Corresponds to Fig. 8 of [2, 3].

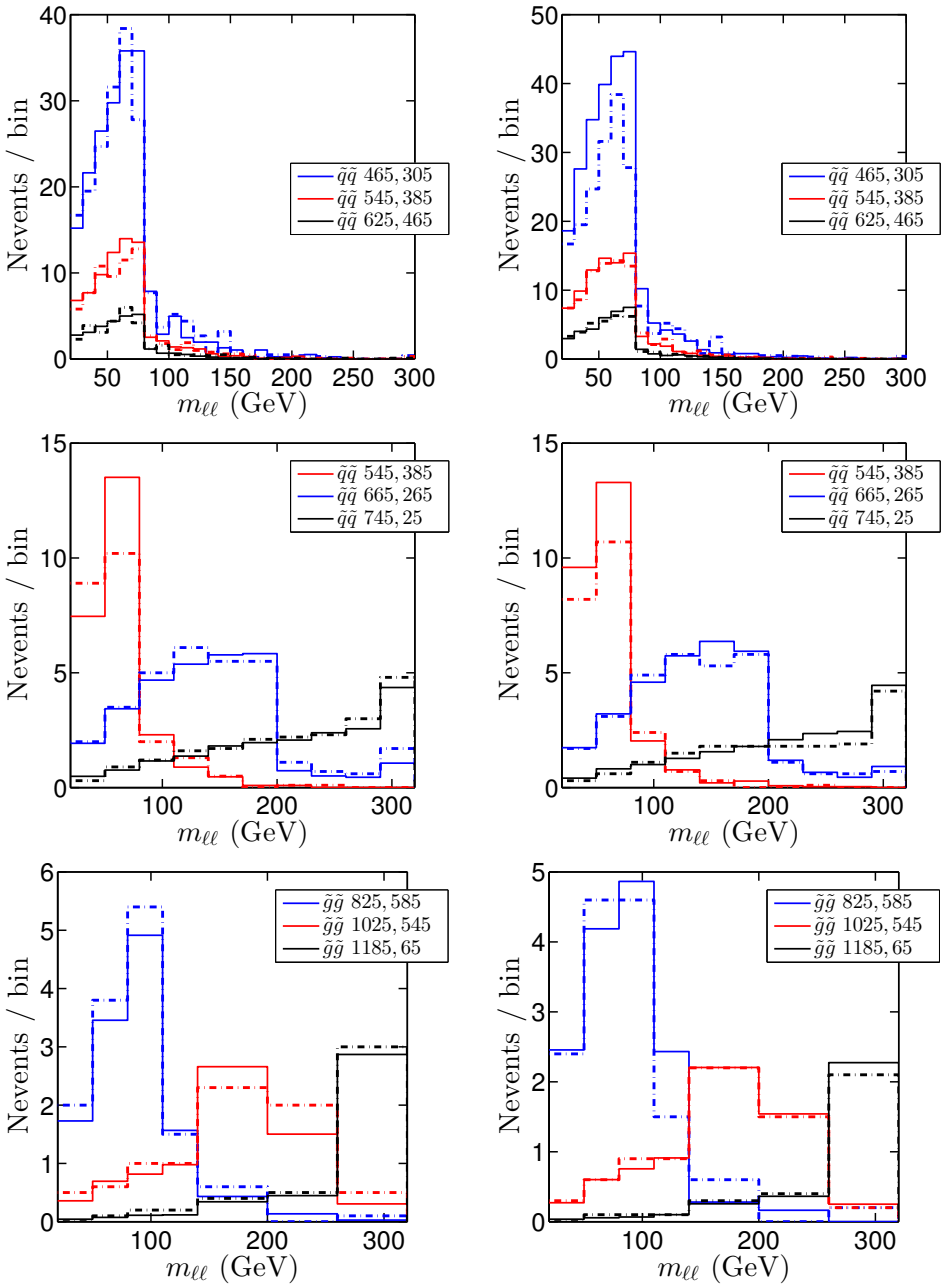

Figure 4: $m_{\ell\ell}$ distributions in the ee (left) and $\mu\mu$ (right) channels, for the SRs SR-loose (top row), SR-2j-bveto (middle row), and SR-4j-bveto (bottom row), after all cuts except the final cut on $m_{\ell\ell}$. Corresponds to Fig. 9 of [2, 3]. Note that, in the experimental publication, the signal line $(625, 545, 505, 465)$ present in the top row is mislabeled as $(665, 465, 365, 265)$ [5].